Investigation of Velocity and Droplet Size Distributions of Flash Boiling LN2-Jets With Phase Doppler Anemometry

Andreas Rees[1*], Lucio Araneo[2], Heiko Salzmann[1], Eldin Kurudzija[1], Dmitry Suslov[1], Grazia Lamanna[3], Joachim Sender[1] and Michael Oschwald[1]
[1]German Aerospace Center (DLR), Institute of Space Propulsion, Langer Grund, 74239 Hardthausen, Germany
[2]Politecnico di Milano, Energy Department, Via Lambruschini 4A, 20156 Milano, Italy
[3]University of Stuttgart, Institute of Aerospace Thermodynamics, Pfaffenwaldring 31, 70569 Stuttgart, Germany
*Corresponding author: andreas.rees@dlr.de

Abstract
For a detailed experimental investigation of superheated cryogenic fluids the new cryogenic test bench M3.3 with a temperature controlled injection system was built at the DLR Institute of Space Propulsion in Lampoldshausen. After a first test campaign with high-speed shadowgraphy of flash boiling liquid nitrogen sprays a Phase Doppler Anemometry system was set-up to investigate the dependence of droplet velocities and diameters on the injection conditions at different positions in the spray. The local velocity distributions show their maximums close to the injector exit before they decrease to values around zero. The droplet diameters show an evolution from bigger structures with an inhomogeneous distribution close to the injector to a monodisperse spray with increasing axial and radial distances. Two droplet populations with different mean velocities were found at most of the spray positions.

Keywords
flash boiling, cryogenic, atomization, spray, Phase Doppler

Introduction

Technology development for propulsion systems of upper stages like the cryogenic Ariane 6 upper stage engine Vinci or for future cryogenic thrusters in reaction control or orbital and maneuvering systems is driven by the invention of new, green propellants to substitute hydrazine, and by new ignition technologies like laser ignition [11]. At high-altitude conditions prior to ignition the liquid propellants are injected into the combustor at near-vacuum conditions. This means that the ambient pressure p_∞ is lower than the liquid's saturation pressure $p_{sat}(T_{inj})$ at the injection temperature T_{inj}. The sudden pressure drop at injection leads to a superheated liquid in a metastable thermodynamic state. The injection of a liquid like that results in a fast expansion and eruptive evaporation, a process called flash boiling or flash evaporation. The evaporating gases raise the pressure inside the combustion chamber until the equilibrium pressure shortly before ignition is reached. To know the composition of the propellants in the combustion chamber related to phase, species and temperature distribution is important for both to determine the parameters for a successful ignition and to avoid destructive pressure peaks.

Flash boiling

The dominating parameters for the flash boiling phenomenon in a given liquid are the injection temperature T_{inj} and the back pressure p_{c}, which can be a near-vacuum chamber pressure or atmospheric conditions. According to figure 1 they both define the degree of superheat of the injected liquid in terms of the pressure ratio

$$R_{\text{p}} = \frac{p_{\text{sat}}(T_{\text{inj}})}{p_{\text{c}}} \tag{1}$$

with the saturation pressure $p_{\text{sat}}(T_{\text{inj}})$ at the injection temperature T_{inj} and the chamber pressure p_{c}. A superheated liquid jet with a high degree of superheat is atomized close to or already in the injector nozzle due to vaporization and produces a fine spray with a big opening angle and small droplets. The influence of aerodynamical processes on the primary atomization can be neglected in this kind of jets [23]. The vaporization and expansion of a flash boiling spray leads to a cool-down to reach a new equilibrium state at the saturation temperature $T_{\text{sat}}(p_{\text{c}})$. These non-equilibrium processes are quite complex and need experimental data for further modelling.

State of research

Flash boiling is observed and investigated since the beginning of the 20$^{\text{th}}$ century [12, 20]. In the last three decades there have been increased efforts of the automotive industry to investigate flash boiling processes of storable liquids typical for the injection into gasoline or diesel engines [1, 2, 6, 17, 18]. Pre-heating the fuel to reach the superheated condition causes flash boiling during the injection which leads to a finer and wider atomization in the combustion chamber. This increases the efficiency and reduces exhaust emissions [18]. Compared with cavitation in the injector nozzle flash boiling was found to be the dominant process for the fuel atomization [1]. Adding small amounts of low boiling liquids to the actual fuel can be used to improve atomization by flash boiling [6]. Hydrocarbon sprays

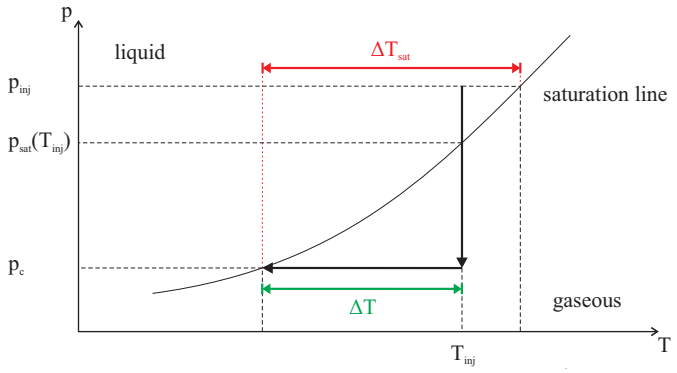

Figure 1. Phase diagram of a superheated liquid for adiabatic depressurization

with dissolved air were investigated by means of Phase Doppler Anemometry (PDA) and showed similar features like flash boiling sprays [2]. First models were developed for flash boiling hydrocarbon sprays to predict the nucleation rates and resulting droplet sizes [17] and for water sprays to predict the liquid superheat with the help of the depressurization transient [5]. Further studies about flash boiling processes can be found concerning the safety field in process technology or chemical and nuclear industry, where storable fluids like hydrocarbons, water, ethanol or refrigerants like R-134A were used [3, 5, 16, 19, 22]. It was found that not only the degree of superheat determines the intensity of flash boiling but also injection conditions like the injection pressure or the injector diameter [22]. By the means of shadowgraphy a remaining liquid core in flash boiling sprays was visualized, where the jet break-up due to phase change takes place in a radial direction [16, 19]. Transition correlations depending on the dimensionless Weber and Jakob numbers were empirically developed for superheated water leaking into the atmosphere to subdivide the resulting sprays into an aerodynamical break-up region, a transition region and a fully flashing region [3, 21]. The validity range of these correlations was successfully expanded for the fluids iso-octane, acetone and ethanol [9]. In the same study the onset criterion χ, which links flash boiling with the classical nucleation theory, for the flashing regimes was developed and a model for predicting the spray angle in the near-nozzle region by the degree of superheat and the dimensionless surface tension was generated. In contrast to storable fluids, flash boiling of cryogenic liquids is much less investigated due to significantly harder experimental conditions. Within an experimental study at DLR Lampoldshausen about laser ignition in a model rocket combustion chamber at high-altitude conditions flash boiling was observed for a liquid oxygen (LOX) jet [4]. Due to a co-flow by gaseous hydrogen the spray angles however were quite narrow for flash boiling sprays. At the same test bench flash boiling of LOX jets with two injection configurations was investigated and the results were compared to flash boiling sprays of storable fluids [8]. Despite the huge differences in their physical properties the LOX sprays and the sprays with storable liquids showed a similar spray morphology. The used injection system, however, was limited in terms of controlling and adjusting the injection temperature. In another experimental study about cryogenic flash boiling, sprays of liquid nitrogen (LN2) for injection times of about 10 s were observed with high-speed shadowgraphy for different injection conditions and injector geometries [10]. The resulting sprays showed maximum spray angles of about 140° and the injector geometry and injection pressure did not have big influences on the spray angles. Furthermore, a solidification of nitrogen was observed. Temperature measurements along the spray axis yielded a cool-down of the sprays below the triple point. In [13] the validity range of the transition correlations from [3, 21] was successfully expanded for the cryogenic fluid LN2 and an asymptotical evolution of the spray angle with increasing superheat was shown. Furthermore, in this study a preliminary PDA measurement campaign showed decreasing droplet diameters with increasing injection temperatures in fully flashing LN2 sprays and a global minimum in the vertical velocity profile as a function of the injection temperature.

Since the dominating parameters for flash boiling are the injection temperature T_{inj} and the back pressure p_{c}, it is important for an experimental investigation to make them adjustable, to keep them constant during the injection period and to make them reproducible. Especially adjusting and controlling the temperature was partly limited in the few studies with cryogenic flash boiling. This is why the new test bench M3.3 with a temperature controlled injection system was built at DLR Lampoldshausen for a detailed experimental investigation of cryogenic flash boiling processes [14, 15].

Experimental set-up

Test bench M3.3

The test bench M3.3 consists of three main systems, as depicted in figure 2: the media supply and pressurization system, the cryogenic temperature adjustment and injection system (CTAIS) and the vacuum system. With the first system all gases (nitrogen, helium, oxygen) for the operation of the test bench are provided and are pressurized with various pressure reducers to the desired pressures. The second of the three main systems consists of a double-walled and vacuum-insulated pressure tank filled with liquid and gaseous nitrogen (GN2), see figure 2 on the left and right. By an evacuation or pressurization of the GN2 phase in the pressure tank the fluid is cooled down or heated up, respectively. In the first case a new saturation state is reached due to vaporization of a certain amount

of LN2. The latent heat of vaporization necessary for this phase change leads to a loss of heat of the liquid/gaseous nitrogen and consequently to a temperature decrease. In the second case the saturation state after pressurization with GN2 is reached due to condensation of the liquid phase. In this process the latent heat of vaporization is released and heats the nitrogen. Inside the pressure tank is the complete LN2/LOX feed and injection system, which consists of a 0.5 L LN2/LOX run-tank, a mass flowmeter, the injector unit with a pneumatic run valve and the injector nozzle, and piping in-between, see figure 2 in the middle. That means that all these sub-systems are completely surrounded by the cooling medium nitrogen to provide a homogeneous temperature distribution from the run-tank to the injector nozzle. Several dynamic pressure and temperature sensors are installed at the nitrogen pressure tank as well as at the feed and injection system, in order to both control and adjust the temperature of the cooling medium and to measure the injection parameters of the injected jets. The latter is realized by a Pt100A temperature sensor and a dynamic pressure sensor 601A by Kistler each installed about 30 mm upstream of the injector nozzle exit. A hand hole at the top of the pressure tank provides the feedthroughs for the sensors and the supply pipes for LN2, GN2 and Helium. The latter is used to pressurize the pneumatic axial run valve (Axius by Stöhr Armaturen) as well as the cable ducts for the sensor cables inside the pressure tank. The CTAIS is mounted on top of the vacuum system, which is a cylindrical chamber with an inner diameter of 300 mm, a height of 225 mm from the injector nozzle exit to the bottom of the chamber and four optical accesses with a diameter of 100 mm each. The four windows are positioned with an angle of 90° to each other. An attached vacuum pump with a pumping speed of 87.5 m^3/h produces the near-vacuum atmosphere to simulate high-altitude conditions. After evacuating all of the pipes and vessels of the CTAIS the system is chilled-down in about 90 minutes by filling it with LN2. During the chill-down the run-tank is filled with the gaseous test fluid, which is nitrogen for the current study. The test fluid gets liquified within this chill-down process. In this study a single injector with a diameter of $D_{\text{inj}} = 1$ mm and a length-to-diameter ratio $L/D = 2.9$ was used.

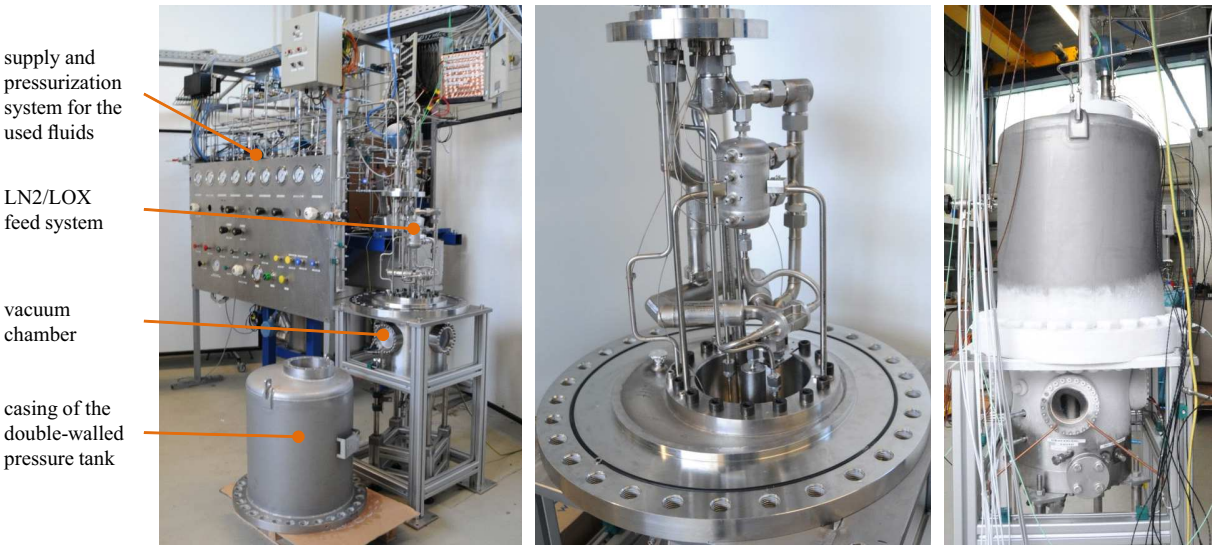

Figure 2. Test bench M3.3 with supply and pressurization system, open CTAIS and vacuum system (left); open CTAIS with run tank, pneumatic run valve, injector unit and sensoric in-between (middle); chilled-down test bench M3.3 in operation mode (right)

The CTAIS allows variable injection conditions, which are summarized in table 1. In the first run-in tests it was shown that the system is capable of keeping the injection temperature T_{inj} constant during the whole injection time of about 2 s, that the injection temperature is reproducible in the range of ± 0.6 K for each test run and that the temperature distribution is homogeneous in the whole test fluid feed line [13, 14].

Table 1. Possible injection conditions of test bench M3.3

parameter	range	unit
injection temperature T_{inj}	75 - 120	K
injection pressure p_{inj}	1 - 20	10^5 Pa
back pressure p_{c}	30 - 1000	10^2 Pa
injector diameter D_{inj}	1 - 2	10^{-3} m
mass flow $\dot{m}$	0.08 - 50	g/s

Optical diagnostics
High-speed shadowgraphy

In a first test campaign high-speed backlight shadowgraphy was used to visualize the injected LN2 sprays. With a xenon light source the sprays were illuminated from the backside through one of the four optical accesses of the vacuum chamber. A translucent milk glas screen was placed between the light source and the chamber window to provide a homogeneous background. The high-speed camera is positioned on the opposite optical access of the chamber. The optical set-up is shown schematically in figure 3 and the used components are listed in table 2. The high-speed camera was set to 10 000 fps with a frame size of 1024×1024 pixels.

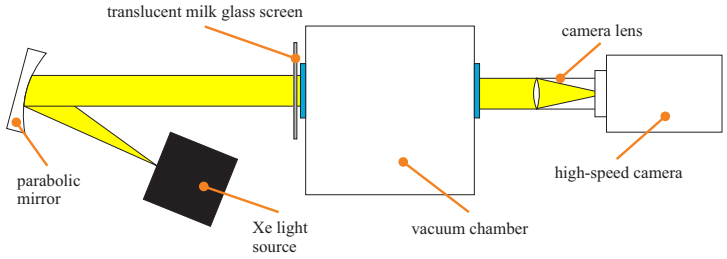

Figure 3. Scheme of the optical set-up for high-speed backlight shadowgraphy at test bench M3.3

Table 2. Components of optical shadowgraphy set-up at test bench M3.3

component	manufacturer	type
xenon light source	Müller Elektrik & Optik	SVX 1450 & LAX 1450
camera lense	Tamron	A061 AF28-300mm
camera	Photron	Fastcam SA-X

Phase Doppler Anemometry

After the preliminary PDA campaign in the dual-mode configuration presented in [13] the Dantec PDA system was set up in the 2D fiber configuration. The optical set-up is depicted in figures 4 (left) and 5 and the main components of the used PDA system are summarized in table 3. Because of the geometrical limited optical access to the spray, both, the transmitter and receiver probes were tilted and positioned with an off-axis angle of $\varphi = 7°$ and 5°, respectively, to use forward scattering first order refraction at a total off-axis angle of $\varphi = 12°$. Tilting both probes and chosing the total off-axis angle of $\varphi = 12°$ provides an optimal compromise between the geometrical field of view and the dominant refraction mode. The field of view determines the matrix of measurement positions, which are shown in figure 4 on the right. Both DPSS lasers were set to a power of about 40 mW which results in a power of approximately 9 mW for each laser beam in the measurement volume. A spatial filter with a slit of 100 µm was chosen. The PDA system was first adjusted and aligned with the help of a water spray produced by a similar nozzle like the injector nozzle in the CTAIS. A needle with a diameter of 1 mm was placed in the injector nozzle of the CTAIS and was illuminated by one of the laser beams to align the traverse horizontally. For its vertical alignment the lower edge of the injector nozzle was used. The refractive index for nitrogen was set to 1.205 according to an interpolation of values derived from [7] in respect to the current wavelengths and to the temperature range for this measurement campaign. With this PDA system the vertical and horizontal droplet velocity as well as the droplet size distributions were measured at different radial and axial locations in fully flashing sprays at constant injection conditions. Based on the optical set-up of the PDA system, droplets with a maximum particle diameter of 83.2 µm can be measured. The velocity ranges were set to $-67\,\text{m/s} \leq U \leq 203\,\text{m/s}$ for the vertical velocity component and to $-160\,\text{m/s} \leq V \leq 241\,\text{m/s}$ for the horizontal one. The maximum statistical errors can be quantified with $\Delta U = \pm 6.1\,\text{m/s}$, $\Delta V = \pm 8.0\,\text{m/s}$ and $\Delta D = \pm 3.3\,\mu\text{m}$ and occur mainly at measurement positions close to the nozzle exit. The detected signals are evaluated and arithmetically averaged for a time period of $t = 120$ to 220 ms after injection start due to steady state injection conditions in this interval.

Table 3. Components of optical PDA set-up at test bench M3.3

component	specification
two DopplerPower DPSS lasers	1 W each; 488 nm and 514 nm wavelength
2D transmitter probe	$D = 60$ mm; 2.2 mm beam diameter; $\varphi = 7°$
2D fiber PDA receiver probe	$D = 112$ mm; $\varphi = 5°$
two front lenses	500 mm focal length; 93 mm aperture
burst processor P800-2D	
2D traverse system	

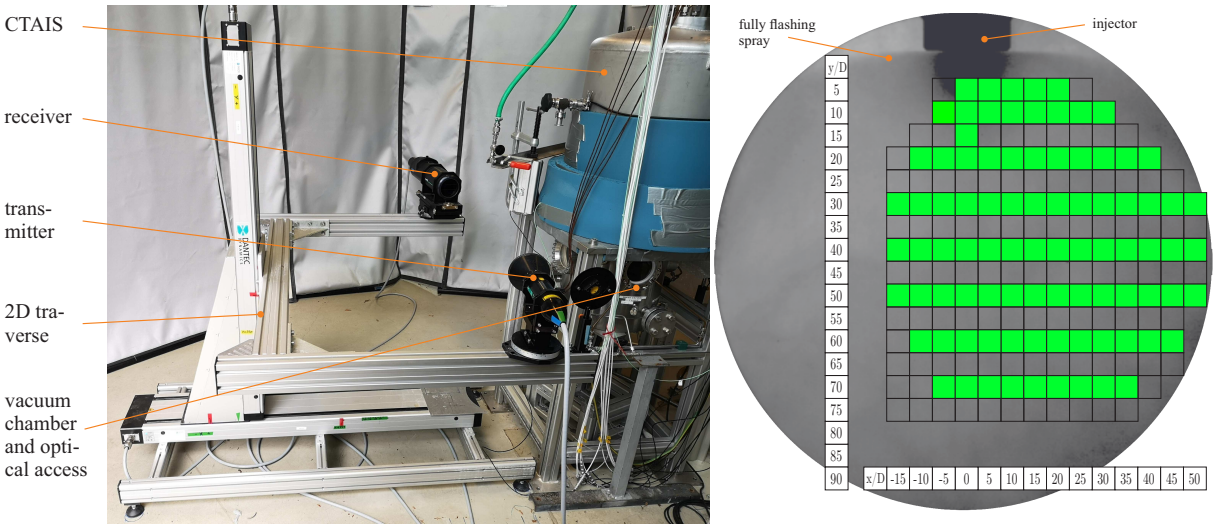

Figure 4. 2D Fiber PDA system at test bench M3.3 (left) and measurement positions in a fully flashing LN2 spray (right)

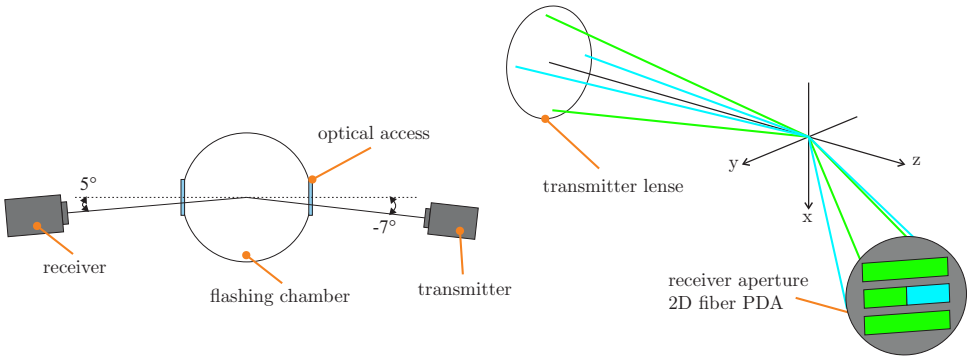

Figure 5. Optical set-up of 2D Fiber PDA system at test bench M3.3 (left) and receiver aperture of the used 2D fiber configuration (right)

Results and discussion

In this study only fully flashing LN2 sprays with injection conditions summarized in table 4 were measured with the PDA system. For each position of the PDA position matrix, one single injection event for a duration of 12 s was studied and the data recorded, synchronized by the valve opening signal. The distributions of the resulting

Table 4. Injection conditions of measured fully flashing LN2 sprays

parameter	value	uncertainty
injection temperature T_{inj}	89.7 K	$\pm$0.6 K
injection pressure p_{inj}	4.4×10^5 Pa	$\pm 0.4 \times 10^5$ Pa
back pressure p_{c}	73×10^2 Pa	$\pm 27 \times 10^2$ Pa
degree of superheat R_{p}	60	$\pm$30

arithmetical mean vertical velocity U, horizontal velocity V and droplet diameter D_{10} are depicted in figure 6 for all the positions defined by the test matrix in figure 4 on the right. Close to the injector exit very high vertical velocities of about 65 m/s were measured, compared to the velocity in the injector of approximately 18 m/s derived from mass flow measurements in the feed lines. However, with increasing distance from the injector nozzle the vertical velocity decreases, especially close to the spray axis, to values about or even slightly less than zero. The latter means that far downstream of the injector nozzle the measured droplets seem to move upwards in some kind of recirculation zones. An indication of such zones is shown in figure 7 and highlighted by the yellow boxes at a constant position in the four shadowgraphy frames of a fully flashing LN2 spray at a time step of 1 ms. The injection conditions with an injection temperature of $T_{\text{inj}} = 90.5$ K, an injection pressure of $p_{\text{inj}} = 5.5 \times 10^5$ Pa and a degree of superheat $R_{\text{p}} = 69$ are similar to the sprays measured by PDA in this study. The dark structure close to the upper edge of the yellow box is nearly motionless or is even slightly floating upstream. With an increasing radial distance from the spray axis the vertical velocities are decreasing as well. This effect is more dominant for y/D-positions closer to the injector than at the positions further downstream. Except for the spray positions close to the injector exit, where the measured horizontal velocity components are roughly around $\pm$20 m/s, the horizontal velocity is close to zero in

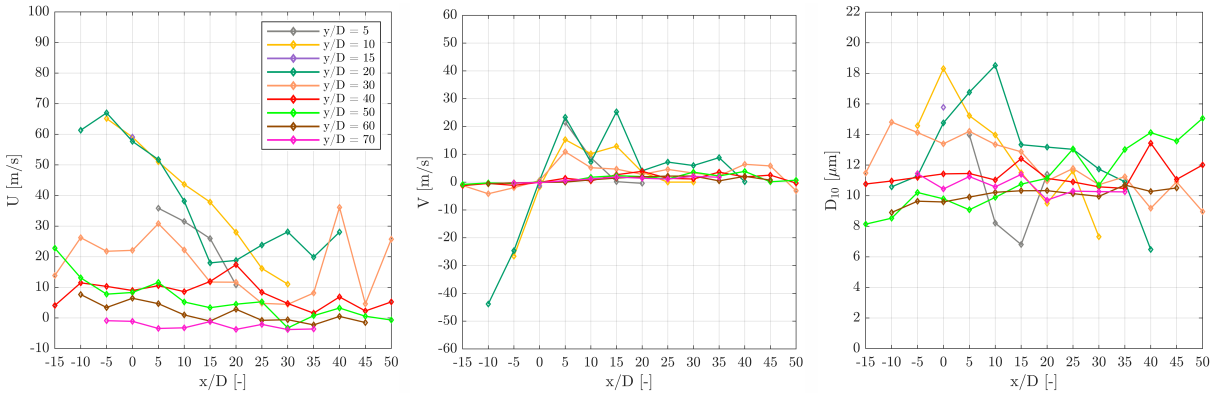

Figure 6. Arithmetical mean vertical and horizontal velocity U (left) and V (middle) and arithmetical mean diameter D_{10} (right) distributions in fully flashing LN2 sprays at $T_{\text{inj}} = 89.7\,\text{K}$ and $p_{\text{inj}} = 4.4 \times 10^5\,\text{Pa}$

large parts of the fully flashing LN2 sprays. This means that close to the injector nozzle at $y/D < 30$ and $|x/D| < 10$ a region with a high kinetic energy exists. Here the internal energy in terms of superheat is partially transformed into kinetic energy by evaporation of the bulk liquid, the break-up of the jet and a fast expansion of the resulting droplets in vertical and horizontal directions.

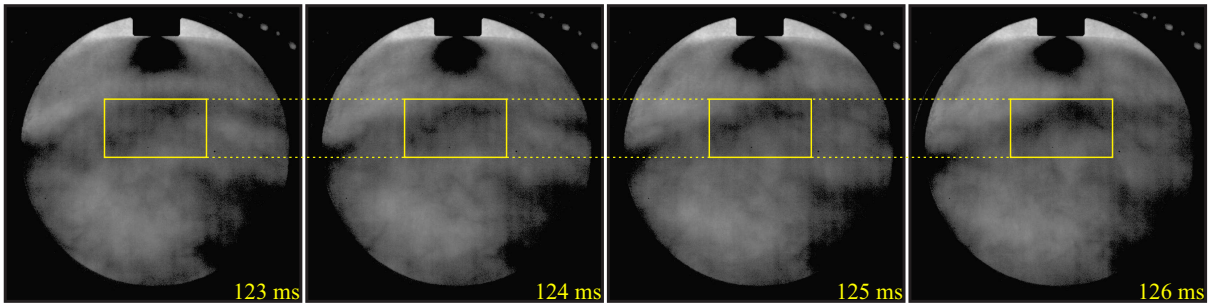

Figure 7. Fully flashing LN2 spray at different times after injection start at $T_{\text{inj}} = 90.5\,\text{K}$, $p_{\text{inj}} = 5.5 \times 10^5\,\text{Pa}$ and $D_{\text{inj}} = 1.0\,\text{mm}$

The droplet diameter distribution is less homogeneous compared to the velocity distributions, especially close to the injector exit. In this region bigger droplets and other liquid structures are still present. Furthermore, getting the phase information of the passing droplets to determine their diameter is likely harder in this region because of the higher kinetic energy. Further downstream the diameter distribution is getting smoother with roughly monodisperse droplet diameters of $D_{10} \approx 10\,\mu\text{m}$. With an increasing radial distance x/D to the spray axis, the droplet diameter decreases for positions $y/D < 40$. Further downstream the diameters seem to increase slightly with increasing x/D-positions.

Some asymmetrical or inhomogeneous peaks in the distributions, like e.g. the vertical velocity component at the position $x/D = 40$ and $y/D = 30$, are caused by inhomogeneities in the sprays, by slightly varying injection conditions or by low partical densities during the acquisition time at some measurement positions.

At all positions in the center of the position matrix two distinctive droplet populations with a different niveau of the vertical velocity component are present in each single injection event as shown in figure 8 on the left, exemplarily at the position $x/D = 0$ and $y/D = 30$. One of these droplet groups shows in this test case a mean velocity of about $40\,\text{m/s}$, the other one much lower velocities slightly below zero. This distinctive feature is not present in the horizontal velocity component, which is zero as expected for a measurement position on the spray axis. The dominance of the upper vertical velocity population is decreasing with increasing axial distance y/D to the injector exit until the lower, negative velocity is dominant like for the vertical velocity distribution U at the position $y/D = 70$ in figure 6. Plotting the vertical velocities U as a function of the measured diameter D shows a weak trend towards smaller droplets at the lower, negative vertical velocity and slightly bigger droplets for the droplet population with the higher velocity. For this study the arithmetical mean values of the U-,V- and D_{10}-distributions in figure 6 were determined for the whole set of detected droplets within the evaluation period, i.e. without taking into account the two different velocity populations.

Comparison with analysed shadowgraphs

To compare the local velocity distributions derived from the PDA measurements, the flow field of a fully flashing LN2 spray was determined by tracing of flow structures in a preliminary image analysis of shadowgraph images. The

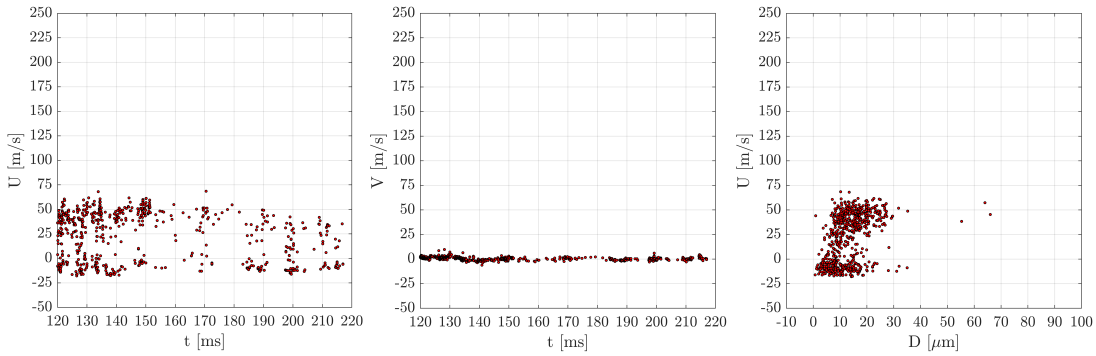

Figure 8. Vertical and horizontal velocities U (left) and V (middle) as functions of arrival time and vertical velocity U as function of the droplet diameter D (right) at position $x/D = 0$ and $y/D = 30$ in fully flashing LN2 sprays at $T_{\text{inj}} = 89.7$ K and $p_{\text{inj}} = 4.4 \times 10^5$ Pa

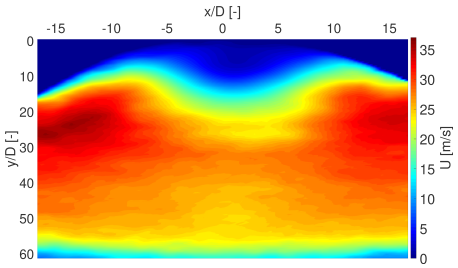

Figure 9. Vertical velocity field for fully flashing LN2 spray by shadowgraphy image analysis

injection conditions of the analysed spray with $T_{\text{inj}} = 82.3$ K, $p_{\text{inj}} = 8.1 \times 10^5$ Pa, $p_c = 150 \times 10^2$ Pa and $R_p = 12$ slightly differ from those used for the PDA campaign. The resulting averaged vertical velocity field is depicted in figure 9. It can be seen, that the maximum velocities occur at axial distances of $y/D \approx 25$ from the injector exit and radial distances of $|x/D| \approx 10$ to 15 from the spray axis. These velocities with values around $36\,\text{m/s}$ are in the same range as the PDA results at these spray positions with respect of the different injection conditions. However, the velocities in the region close to the spray axis are much smaller than the ones determined by PDA. These discrepancies are due to the limited applicability of the image analysing process on fully flashing sprays with mono disperse liquid structures, which also is a reason for chosing injection conditions with a quite low degree of superheat $R_p = 12$ for this analysis. But this preliminary analysis indicates the decrease of the vertical velocity to values close to zero with an increasing axial distance from the injector exit in accordance with the PDA results.

Conclusion and outlook

At the new cryogenic test bench M3.3 with a temperature controlled injection system flash boiling liquid nitrogen sprays were analysed with a Phase Doppler system in 2D fiber PDA configuration to determine the velocity and diameter distributions. For this measurement campaign the injection conditions in terms of temperature, pressure and injector geometry were kept constant while the measurement positions of the PDA system were varied. The local velocity distributions show their maximums close to the injector exit because of a high kinetic energy in that region due to evaporation and expansion of the liquid nitrogen jet. For increasing distances to the injector exit the velocities decrease to values around zero. The droplet diameters show an evolution from bigger structures with an inhomogeneous distribution close to the injector to a monodisperse spray with increasing axial and radial distances. The observed two droplet populations with different mean velocities will be analysed separately and a detailed comparison with shadowgraph images has to be done to understand these two populations. The purpose of the test campaigns with LN2 is not only to provide a detailed data base about flash boiling LN2 sprays for numerical modelling and validation but also to prepare the investigation of flash boiling of the actual rocket propellants like liquid oxygen in the near future or liquid methane later on at this test bench.

Acknowledgements

The authors acknowledge funding received from the DFG within the SFB TRR75. The authors thank Johann Fröse, Markus Dengler, Artur Walz-Steinbach and Michael Zepmeisel for their support at the M3.3 test bench before and during the test campaigns. Furthermore, the authors thank Marek Czapp and Max Frederik Luh for their assistance with setting up and aligning the PDA system.

Nomenclature

χ	onset criterion [-]	D	diameter [mm]
φ	off-axis angle [°]	D_{10}	arithmetical mean diameter [µm]

L	length [m]	x	horizontal direction [mm]
p	pressure [Pa]	y	vertical direction [mm]
R_p	degree of superheat [-]	**Subscripts**	
T	temperature [K]	∞	ambient condition
t	time [ms]	c	chamber condition
U	vertical velocity component [m/s]	inj	injection condition
V	horizontal velocity component [m/s]	sat	saturation condition

References

[1] Aleiferis, P.G., J. Serras-Pereira, A. Augoye, T.J. Davies, R.F. Cracknell, and D. Richardson. Effect of Fuel Temperature on In-Nozzle Cavitation and Spray Formation of Liquid Hydrocarbons and Alcohols from a Real-Size Optical Injector for Direct-Injection Spark-Ignition Engines. *Int. J. Heat Mass Transfer*, 53(21-22):4588–4606, 2010.

[2] Araneo, L. and R. Dondè. Atomization of a G-DI Spray with Air Dissolved in Gasoline and Mono-component Fuels. In *29th ILASS-Europe Conference*, Paris, France, September 2019.

[3] Cleary, V., P. Bowen, and H. Witlox. Flashing Liquid Jets and Two-Phase Droplet Dispersion: I. Experiments for Derivation of Droplet Atomisation Correlations. *J. Hazard. Mater.*, 142(3):786–796, April 2007.

[4] De Rosa, M., J. Sender, H. Zimmermann, and M. Oschwald. Cryogenic Spray Ignition at High Altitude Conditions. In *42nd AIAA/ASME/SAE/ASEE JPC*, Sacramento, California, July 2006.

[5] Elias, E. and P.L. Chambré. Flashing Inception in Water During Rapid Decompression. *J. Heat Transfer*, 115(1):231–238, February 1993.

[6] Gemci, T., K. Yakut, N. Chigier, and T.C. Ho. Experimental Study of Flash Atomization of Binary Hydrocarbon Liquids. *Int. J. Multiph. Flow*, 30(4):395–417, 2004.

[7] Johns, H.E. and J.O. Wilhelm. The Refractive Indices of Liquid Oxygen, Nitrogen, and Hydrogen. *Can. J. Res.*, 15(7):101–108, July 1937.

[8] Lamanna, G., H. Kamoun, B. Weigand, C. Manfletti, A. Rees, J. Sender, M. Oschwald, and J. Steelant. Flashing Behavior of Rocket Engine Propellants. *At. Spray*, 25(10):837–856, 2015.

[9] Lamanna, G., H. Kamoun, B. Weigand, and J. Steelant. Towards a Unified Treatment of Fully Flashing Sprays. *Int. J. Multiph. Flow*, 58:168–184, 2014.

[10] Luo, M. and O.J. Haidn. Characterization of Flashing Phenomena with Cryogenic Fluid Under Vacuum Conditions. *J. Propul. Power*, 3(5):1253–1263, May 2016.

[11] Manfletti, C. Laser Ignition of an Experimental 400N Cryogenic Reaction and Control Thruster: Pre-Ignition Conditions. *Journal of Propulsion and Power*, 30(4):925–933, July-August 2014.

[12] Meyer, J. Zur Kenntnis des negativen Drucks in Flüssigkeiten. *Abh. Dtsch. Bunsen-Ges. Phys. Chem.*, 3(1):1–53, 1911.

[13] Rees, A., H. Salzmann, J. Sender, and M. Oschwald. Investigation of Flashing LN2-Jets in Terms of Spray Morphology, Droplet Size and Velocity Distributions. In *8th EUCASS*, Madrid, Spain, July 2019.

[14] Rees, A., J. Sender, and M. Oschwald. Cryogenic Flash Boiling in Liquid Rocket Engines. In *IICR 5th Cavitation Workshop*, Chania, Crete, June 2017.

[15] Rees, A., J. Sender, and M. Oschwald. Temperature Dependence of Flashing LN2-Jets. In *Space Propulsion Conference*, Seville, Spain, May 2018.

[16] Reitz, R.D. A Photographic Study of Flash-Boiling Atomization. *Aerosol Sci. Technol.*, 12(3):561–569, 1990.

[17] Senda, J., Y. Hojyo, and H. Fujimoto. Modeling on Atomization and Vaporization Process in Flash Boiling Spray. *JSAE Review*, 15(4):291–296, 1994.

[18] Senda, J., Y. Wada, D. Kawano, and H. Fujimoto. Improvement of Combustion and Emissions in Diesel Engines by Means of Enhanced Mixture Formation Based on Flash Boiling of Mixed Fuel. *Int. J. Engine Res.*, 9(1):15–27, 2008.

[19] Simões-Moreira, J.R., M.M. Vieira, and E. Angelo. Highly Expanded Flashing Liquid Jets. *J. Thermophys. Heat Transfer*, 16(3):415–424, 2002.

[20] Wismer, K.L. The Pressure-Volume Relation of Super-heated Liquids. *J. Phys. Chem.*, 26(4):301–315, June 1921.

[21] Witlox, H., M. Harper, P. Bowen, and V. Cleary. Flashing Liquid Jets and Two-Phase Droplet Dispersion: II. Comparison and Validation of Droplet Size and Rainout Formulations. *J. Hazard. Mater.*, 142(3):797–809, April 2007.

[22] Yildiz, D., P. Rambaud, J. Van Beeck, and J.-M. Buchlin. A Study on the Dynamics of a Flashing Jet. Final Contract Research Report EAR0030, VKI, 2002.

[23] Zeng, Y. and C.-F.F. Lee. An Atomization Model for Flash Boiling Sprays. *Combust. Sci. and Tech.*, 169(1):45–67, 2001.